**Astronomy
&
Astrophysics**

The Milky Way Cepheid Leavitt law based on *Gaia* DR2 parallaxes of companion stars and host open cluster populations

Louise Breuval[1], Pierre Kervella[1], Richard I. Anderson[2], Adam G. Riess[3,4], Frédéric Arenou[5], Boris Trahin[1], Antoine Mérand[2], Alexandre Gallenne[6,7,8,9], Wolfgang Gieren[7], Jesper Storm[10], Giuseppe Bono[11,12], Grzegorz Pietrzyński[7,8], Nicolas Nardetto[6], Behnam Javanmardi[1], and Vincent Hocdé[6]

[1] LESIA, Observatoire de Paris, Université PSL, CNRS, Sorbonne Université, Univ. Paris Diderot, Sorbonne Paris Cité, 5 place Jules Janssen, 92195 Meudon, France
e-mail: louise.breuval@obspm.fr
[2] European Southern Observatory, Karl-Schwarzschild-Str. 2, 85748 Garching, Germany
[3] Space Telescope Science Institute, 3700 San Martin Drive, Baltimore, MD 21218, USA
[4] Department of Physics and Astronomy, Johns Hopkins University, Baltimore, MD 21218, USA
[5] GEPI, Observatoire de Paris, Université PSL, CNRS, 5 place Jules Janssen, 92190 Meudon, France
[6] Université Côte d'Azur, Observatoire de la Côte d'Azur, CNRS, Laboratoire Lagrange, France
[7] Universidad de Concepción, Departamento de Astronomía, Casilla 160-C, Concepción, Chile
[8] Nicolaus Copernicus Astronomical Centre, Polish Academy of Sciences, Bartycka 18, 00-716 Warszawa, Poland
[9] Unidad Mixta Internacional Franco-Chilena de Astronomía (CNRS UMI 3386), Departamento de Astronomía, Universidad de Chile, Camino El Observatorio 1515, Las Condes, Santiago, Chile
[10] Leibniz-Institut für Astrophysik Potsdam (AIP), An der Sternwarte 16, 14482 Potsdam, Germany
[11] Department of Physics, Università di Roma Tor Vergata, Via della Ricerca Scientifica 1, 00133 Roma, Italy
[12] INAF-Osservatorio Astronomico di Roma, Via Frascati 33, 00040 Monte Porzio Catone, Italy

ABSTRACT

Aims. Classical Cepheids provide the foundation for the empirical extragalactic distance ladder. Milky Way Cepheids are the only stars in this class accessible to trigonometric parallax measurements. However, the parallaxes of Cepheids from the second *Gaia* data release (GDR2) are affected by systematics because of the absence of chromaticity correction, and occasionally by saturation.
Methods. As a proxy for the parallaxes of 36 Galactic Cepheids, we adopt either the GDR2 parallaxes of their spatially resolved companions or the GDR2 parallax of their host open cluster. This novel approach allows us to bypass the systematics on the GDR2 Cepheids parallaxes that is induced by saturation and variability. We adopt a GDR2 parallax zero-point (ZP) of -0.046 mas with an uncertainty of 0.015 mas that covers most of the recent estimates.
Results. We present new Galactic calibrations of the Leavitt law in the V, J, H, K_S, and Wesenheit W_H bands. We compare our results with previous calibrations based on non-*Gaia* measurements and compute a revised value for the Hubble constant anchored to Milky Way Cepheids.
Conclusions. From an initial Hubble constant of 76.18 ± 2.37 km s^{-1} Mpc^{-1} based on parallax measurements without *Gaia*, we derive a revised value by adopting companion and average cluster parallaxes in place of direct Cepheid parallaxes, and we find $H_0 = 72.8 \pm 1.9$ (statistical + systematics) ± 1.9 (ZP) km s^{-1} Mpc^{-1} when all Cepheids are considered and $H_0 = 73.0 \pm 1.9$ (statistical + systematics) ± 1.9 (ZP) km s^{-1} Mpc^{-1} for fundamental mode pulsators only.

Key words. parallaxes – stars: distances – stars: variables: Cepheids – distance scale

1. Introduction

Classical Cepheids (CCs) have a historical major importance among variable stars because of the simple correlation between the pulsation period and intrinsic luminosity, also called the Leavitt law or the period–luminosity (PL) relation (Leavitt 1908; Leavitt & Pickering 1912). However, after more than a century of active research, the absolute calibration of the Leavitt law is still unsatisfactory because of the lack of precise and direct distance measurements for a sizeable sample of these stars. A careful calibration of this relation and especially of its zero-point is fundamental as it is used to establish extragalactic distances and to derive the expansion rate of the Universe, the Hubble constant H_0. The determination of H_0 from the cosmic microwave background (CMB) based on the standard Λ cold dark matter (ΛCDM) model (Planck Collaboration VI 2020) is currently found to be in $\sim 5\sigma$ tension with the empirical or direct distance ladder measurements (Riess 2019). This tension may have

important implications in cosmology, and may even point toward new physics beyond ΛCDM (Verde et al. 2019).

Calibrating the Leavitt law requires independent and accurate distance measurement for a sample of CCs. Unfortunately, *Gaia*'s second data release (hereafter GDR2) contains a number of systematic effects that may reduce the precision of the parallaxes of CCs (Gaia Collaboration 2018). First, CCs are bright stars, so a small number with $G < 6$ mag are affected by saturation, making their parallaxes unreliable. In addition, CC colors cycle through many variations during the parallax cycle; the effective temperature of a Cepheid changes on average by 1000 K over a full pulsation cycle (Proxauf et al. 2018), which means ~ 0.5 mag in optical bands, so this may add additional noise to their astrometry due to the chromaticity of the PSF. Future *Gaia* data releases are expected to include chromaticity corrections for variable stars and incorporate a better model of the PSF to deal with saturation. While recent analyses of *Gaia* DR2 parallaxes for CCs with $G > 6$ mag do not appear to be

affected by excess noise (an indicator of poor quality for GDR2 astrometric data; Groenewegen 2018; Riess et al. 2018a; Gaia Collaboration 2017; Clementini et al. 2019), it is important to pursue alternative approaches to extract parallaxes from *Gaia* DR2 for CCs that are insensitive to these systematics.

Even in the absence of systematic errors, the use of open cluster parallaxes for the CCs they host can provide enhanced precision over the use of a single CC parallax. Because open cluster parallaxes are based on many stars, the increased precision from averaging and the ability to reject outliers for stars in astrometric binaries is extremely valuable.

In the present paper our aim is to calibrate the Milky Way (MW) Cepheid Leavitt law using stars that are not affected by these issues and to benefit from the gain in precision afforded by cluster average parallaxes. In Sect. 2 we introduce our sample of stars and their associated parallaxes and photometry. In Sect. 3.1 we derive calibrations of the Leavitt law in various bands. Then in Sect. 3.2 we compare our GDR2 parallaxes with the corresponding expected parallaxes from *Hubble* Space Telescope (HST) measurements, and in Sect. 3.3 we derive a value for the Hubble constant anchored to Milky Way Cepheids.

2. Sample

We consider two sets of parallaxes: one based on Cepheid companions and one based on average cluster parallaxes. The benefits of these samples are flux and color constancy (companions and clusters) and averaging over a large sample (clusters).

2.1. Parallaxes of Cepheid resolved companions

Recently, Kervella et al. (2019) presented a sample of 28 Galactic Cepheids that are members of gravitationally bound and spatially resolved stellar systems. In these systems Cepheid companions are photometrically stable stars and their GDR2 parallaxes are therefore not affected by such a strong chromatic effect as Cepheids. As the CCs and their companions share the same parallax (their relative distance is negligible compared to the distance to *Gaia*), the GDR2 parallaxes of the companions provide a natural proxy for those of the CCs. The companions' parallaxes are precise within 15%, on average. A comparison between direct GDR2 Cepheid parallaxes and the corresponding GDR2 companion parallaxes is displayed in Fig. 1.

The angular separation between the CCs and their companions is in most cases larger than 10 arcsec, which is large enough to prevent flux contamination, given the brightness of the CCs. At 10″ separation for stars hundreds to thousands of parsec distant there is no expected effect of orbital motion on parallax or proper motion measurements: the parallaxes of the CCs and companions are not sensitive to the binarity of these wide systems.

The GDR2 astrometry is generally of poor quality for very bright stars ($G < 6$ mag), due to calibration issues and saturation (Riess et al. 2018a; Drimmel et al. 2019; Lindegren 2020). This occurs independently of the chromaticity issue raised previously, whether the star is variable or not. While several Cepheids in our sample are close to this limit, with an average G magnitude of 8 mag, their companions are on average 7 mag fainter than their parent Cepheids. The companions are therefore not as affected as CCs by the saturation issue and they are far away from the sensitivity limit. They consequently belong to the best dynamical range for *Gaia*.

For a given Cepheid, when more than one companion was found by Kervella et al. (2019), we selected the companion with the smallest uncertainty on its parallax. This selection was performed for CV Mon, SY Nor, U Sgr, and V350 Sgr.
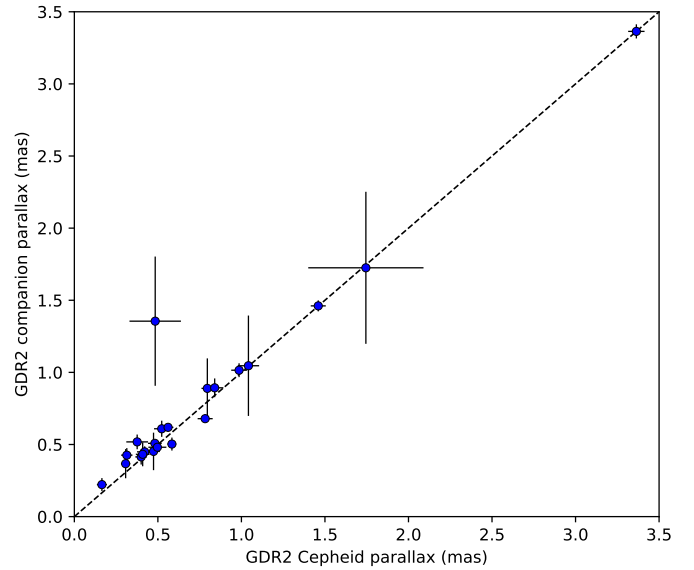

Fig. 1. GDR2 parallaxes of our sample of companions as a function of the corresponding GDR2 Cepheid parallax. The dashed line corresponds to the identity line.

Various quality indicators are introduced in the second release of *Gaia* data, such as the re-normalized unit weight error (RUWE, noted ϱ in the following). It is particularly pertinent because it evaluates the quality of the parallax of a star compared to other stars of the same type. This parameter is defined by Lindegren (2018a) as

$$\varrho = \frac{\text{UWE}}{u_0(G, C)}, \tag{1}$$

where UWE $= \sqrt{\chi^2/(N-5)}$ is the unit weight error and u_0 is an empirical normalization factor that is not directly available in the *Gaia* release, but which can be computed from the lookup table on the ESA DR2 *Known issues* web page[1]. Following Lindegren (2018a), we estimate that a parallax is reliable if $\varrho < 1.4$. The Table 1 gives the RUWE for the Cepheids and the companions in our sample.

We note that some CCs from the Kervella et al. (2019) sample have no valid GDR2 parallax (δ Cep, R Cru, α UMi), while all companions have a valid parallax. In the initial Kervella et al. (2019) sample of 28 Cepheids, five of them have $\varrho > 1.4$, while only two companions are in this case, R Cru and V1046 Cyg, with $\varrho = 2.80$ and 1.51, respectively. We exclude these two stars from the sample of companions in order to keep accurate parallaxes only. The star CE Cas B is a particular case because its companion CE Cas A is also a Cepheid. We exclude both stars from our sample as a precaution.

The star α UMi is extremely bright, with $K \approx 0.5$ mag. Therefore, measuring accurate photometry for this star is particularly challenging. It has no valid parallax in GDR2 and appears saturated in most catalogs (Skrutskie et al. 2006). The only accurate average magnitudes based on several pulsation cycles were found in the AAVSO database that provides $J = 0.93 \pm 0.01$ mag and $H = 0.67 \pm 0.01$ mag in the UKIRT system. Additionally, the uncertain pulsation mode and the age difference between the Cepheid and its companion raise questions concerning the properties of α UMi and whether it should be included in PL relation fits (Anderson 2018; Bond et al. 2018;

---

[1] https://www.cosmos.esa.int/web/gaia/dr2-known-issues

Table 1. Sample of Cepheids in resolved binary systems taken from [Kervella et al. (2019)](#): parameters of the Cepheids and of their stable companions.

Cepheid	ϖ_{GDR2} (mas)	ϱ	G (mag)	BP–RP (mag)	Companion (GDR2)	ϖ_{GDR2} (mas)	ϱ	G (mag)	BP–RP (mag)
DF Cas	$0.307_{\pm 0.028}$	0.98	10.43	1.50	465719182408531072	$0.367_{\pm 0.101}$	1.12	17.26	2.02
CM Sct	$0.376_{\pm 0.065}$	1.02	10.51	1.81	4253603428053877504	$0.518_{\pm 0.051}$	0.95	14.73	1.49
EV Sct	$0.497_{\pm 0.054}$	1.05	9.62	1.63	4156513016572003840	$0.481_{\pm 0.034}$	1.03	13.62	0.88
TV CMa	$0.314_{\pm 0.034}$	0.94	10.08	1.69	3044483895574944512	$0.426_{\pm 0.049}$	1.12	15.77	1.18
V532 Cyg	$0.561_{\pm 0.032}$	0.86	8.67	1.44	1971721839529622272	$0.619_{\pm 0.027}$	0.93	14.67	1.04
V950 Sco	$0.840_{\pm 0.052}$	1.09	7.05	1.05	5960623340819000192	$0.893_{\pm 0.065}$	1.00	15.28	1.03
V350 Sgr	$0.986_{\pm 0.047}$	0.92	7.25	1.26	4080121319521641344	$1.015_{\pm 0.048}$	0.96	12.27	0.50
VW Cru	$0.783_{\pm 0.045}$	0.98	9.01	1.85	6053622508133367680	$0.679_{\pm 0.028}$	0.96	14.07	1.18
AX Cir	$1.745_{\pm 0.345}$	10.3 (*)	5.63	1.15	5874031027625742848	$1.725_{\pm 0.527}$	1.13	19.82	1.65
δ Cep	–	20.9 (*)	–	–	2200153214212849024	$3.364_{\pm 0.049}$	0.85	6.28	−0.02
CV Mon	$0.482_{\pm 0.041}$	1.16	9.61	1.78	3127142327895572352	$0.508_{\pm 0.025}$	1.03	13.49	1.03
QZ Nor	$0.474_{\pm 0.038}$	1.01	8.58	1.18	5932565899990412672	$0.452_{\pm 0.130}$	1.02	17.93	1.29
V659 Cen	$0.484_{\pm 0.154}$	4.52 (*)	6.39	1.04	5868451109212716928	$1.355_{\pm 0.448}$	1.00	19.69	2.50
CS Vel	$0.165_{\pm 0.030}$	1.01	11.10	1.83	5308893046071732096	$0.222_{\pm 0.045}$	0.95	16.20	1.08
RS Nor	$0.421_{\pm 0.046}$	0.99	9.49	1.73	5932812740361508736	$0.449_{\pm 0.038}$	1.06	14.55	0.97
X Cru	$0.523_{\pm 0.046}$	0.97	8.07	1.28	6059762524642419968	$0.609_{\pm 0.056}$	1.16	16.04	1.11
AW Per	$1.042_{\pm 0.064}$	1.06	7.05	1.97	174489098011144960	$1.046_{\pm 0.348}$	1.07	17.42	1.54
U Sgr	$1.460_{\pm 0.045}$	1.06	6.35	1.54	4092905203841177856	$1.461_{\pm 0.038}$	0.90	11.14	0.67
ER Car	$0.796_{\pm 0.035}$	0.95	6.61	1.08	5339394048386734336	$0.889_{\pm 0.208}$	1.09	18.44	1.37
SX Vel	$0.409_{\pm 0.041}$	1.00	7.97	1.24	5329838158460399488	$0.432_{\pm 0.083}$	0.95	17.02	1.13
SY Nor	$0.400_{\pm 0.035}$	1.10	8.97	1.83	5884729035245399424	$0.414_{\pm 0.053}$	1.28	12.10	0.88
RS Pup	$0.584_{\pm 0.026}$	0.97	6.46	1.88	5546476755539995008	$0.503_{\pm 0.045}$	1.00	16.25	1.28

Notes. The symbol ϱ is the RUWE quality indicator from GDR2 and (*) indicates that $\varrho > 1.4$.

[Groenewegen 2018](#)). We decided to exclude this star from our sample.

Finally, this selection results in a sample of 22 GDR2 parallaxes of Cepheids resolved companions, listed in Table 1.

2.2. Parallaxes of Cepheids in open clusters

Open clusters (OCs) contain a significant number of stars located at the same distance and are numerous in the Milky Way. Therefore, identifying Cepheids in OCs allows us to estimate their distances, with an important gain in precision by taking the average over a population compared to individual parallax measurements.

We performed a cross-match between the [Ripepi et al. (2019)](#) reclassification of GDR2 Cepheids and the [Cantat-Gaudin et al. (2018)](#) catalog of Milky Way Open Clusters. This catalog provides parallaxes for 1229 OCs, computed as the median GDR2 parallax of their member stars. Our comparison is based on five membership constraints: separation θ, parallax ϖ, proper motion μ_α^* and μ_δ, and age.

Following [Anderson et al. (2013)](#), we start the search for potential cluster members by looking at the proximity in the sky: we selected all Cepheids located in a region of $10r_{50}$ around each cluster (where r_{50} is the radius containing half of the members) and we find a total of 2647 couples. For these couples we compared the parallaxes, the proper motions, and the ages of the two components. Since GDR2 parallaxes of Cepheids may be affected by systematics due to the absence of chromaticity correction, we account for this effect by including 20% error in quadrature. The proper motions for Cepheids and open clusters are taken from [Ripepi et al. (2019)](#) and [Cantat-Gaudin et al. (2018)](#), respectively. The age of open clusters is provided by [Kharchenko et al. (2013)](#), and the age for Cepheids is derived using period–age relations from [Anderson et al. (2016)](#).

We also searched in the literature for additional combinations and examined whether they satisfy our membership constraints. Some Cepheids are not present in the [Ripepi et al. (2019)](#) reclassification, so they could not be found by means of our cross-match. [Anderson et al. (2013)](#) presented many of our couples and provided three additional combinations that verify our membership criteria: TW Nor, CV Mon, and V0367 Sct respectively in Lyngå 6, vdBergh 1, and NGC 6649. Other studies, such as [An et al. (2007)](#) and [Chen et al. (2015)](#), also confirm most of our cluster memberships. Recently, [Clark et al. (2015)](#) and [Lohr et al. (2018)](#) identified new Cepheids as potential members of open clusters. However, no near-infrared (NIR) multi-epoch photometry is available for these Cepheids. Moreover, the [Clark et al. (2015)](#) starburst cluster VdBH 222 is not present in the [Cantat-Gaudin et al. (2018)](#) catalog. Therefore, we did not include them in our sample.

We find a total of 14 Cepheids that are candidate members of open clusters. They are listed in Table 2, where filled circles stand for the agreement of a parameter at 1σ or less. In this table is also provided the separation in arcmin between a Cepheid and the center of its host cluster.

Due to the limited angular size of a cluster, parallaxes of the member stars of a same cluster are highly correlated. Uncertainties provided by [Cantat-Gaudin et al. (2018)](#) neglect this effect. Therefore, we revised the open cluster parallax uncertainties by including spatial correlations. We used the approach described in [Lindegren (2018b)](#) and retrieved the spatial covariance $V_\varpi(\theta)$ of parallax errors on the ESA DR2 *Known issues* web page[2]. For each cluster, Table 2 provides the original [Cantat-Gaudin et al. (2018)](#) uncertainties, the number of member stars in each cluster, the cluster radius r_{50}, the averaged $V_\varpi(\theta)$, and the

---

[2] https://www.cosmos.esa.int/web/gaia/dr2-known-issues

Table 2. Sample of cluster Cepheids found by our cross-match selection and in the literature.

Cepheid	Cluster		Cross-match						Cluster parameters			
		ϖ	μ_α^*	μ_δ	Age	Sep (arcmin)	Ref.	$\varpi_{\rm CG18}$ (mas)	$N_{\rm memb}$	r_{50} (deg)	$\langle V_\varpi \rangle$ (μas^2)	$\varpi_{\rm adopted}$ (mas)
CV Mon	vdBergh 1	●	●	●	●	0.9	a, b, c, d	$0.523_{\pm 0.010}$	73	0.03	1741	$0.523_{\pm 0.043}$
S Nor	NGC 6087	●	●	●	●	1.0	a, b, c, e	$1.025_{\pm 0.004}$	251	0.25	708	$1.025_{\pm 0.027}$
U Sgr	IC 4725	●	●	●	●	2.1	a, b, c	$1.514_{\pm 0.003}$	516	0.26	563	$1.514_{\pm 0.024}$
V367 Sct	NGC 6649	●	●	●	●	2.8	a	$0.467_{\pm 0.004}$	560	0.06	1689	$0.467_{\pm 0.041}$
V Cen	NGC 5662	●	●	●	●	25	a, b, c, f	$1.288_{\pm 0.003}$	255	0.33	533	$1.288_{\pm 0.023}$
RS Ori	FSR 0951	●	●	●	2.4 σ	2.0	PW	$0.553_{\pm 0.004}$	195	0.16	697	$0.553_{\pm 0.027}$
CS Vel	Ruprecht 79	●	●	●	2.5 σ	2.2	g	$0.221_{\pm 0.004}$	178	0.05	1720	$0.221_{\pm 0.042}$
DL Cas	NGC 129	●	●	3.4 σ	●	3.4	a, b, c	$0.511_{\pm 0.002}$	392	0.17	904	$0.511_{\pm 0.031}$
EV Sct	NGC 6664	●	1.1 σ	●	●	2.4	a	$0.468_{\pm 0.004}$	237	0.10	1215	$0.468_{\pm 0.035}$
V340 Nor	NGC 6067	●	1.3 σ	●	●	0.9	a, c	$0.443_{\pm 0.002}$	995	0.11	1263	$0.443_{\pm 0.036}$
CF Cas	NGC 7790	●	1.9 σ	●	●	1.3	a, b, c	$0.269_{\pm 0.004}$	200	0.06	1642	$0.269_{\pm 0.041}$
TW Nor	Lyngå 6	●	2.0 σ	●	1.4 σ	0.6	a, b, c, h	$0.383_{\pm 0.006}$	79	0.06	1730	$0.383_{\pm 0.042}$
QZ Nor	NGC 6067	●	1.2 σ	9 σ	●	18	a	$0.443_{\pm 0.002}$	955	0.11	1263	$0.443_{\pm 0.036}$
CG Cas	Berkeley 58	●	4.1 σ	2.0 σ	1.2 σ	5.5	a, b	$0.282_{\pm 0.004}$	142	0.06	1661	$0.282_{\pm 0.041}$

Notes. Full circles stand for an agreement smaller than 1σ between the Cepheid and the cluster parameters.
References. (a): Anderson et al. (2013); (b): Chen et al. (2015); (c): An et al. (2007); (d): Turner et al. (1998); (e): Turner (1986); (f): Turner (1982); (g): Turner (2010); (h): Majaess et al. (2011); (PW): present work.
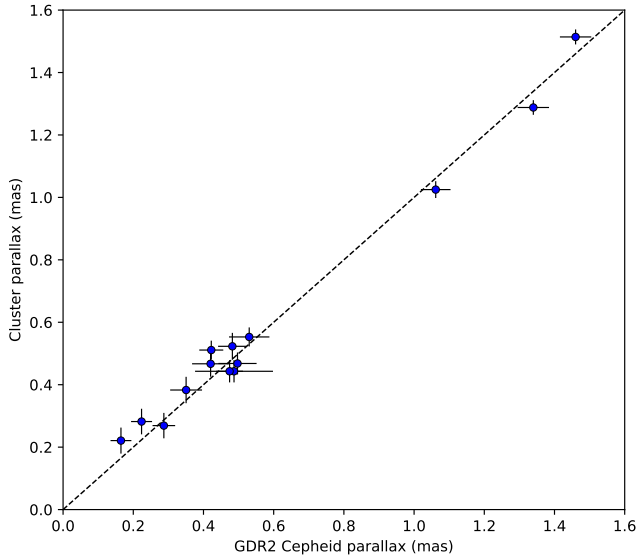

Fig. 2. Parallaxes of our sample of cluster Cepheids from Cantat-Gaudin et al. (2018) with revised uncertainties, as a function of the corresponding GDR2 Cepheid parallax. The dashed line corresponds to the identity line.

adopted parallax $\varpi_{\rm adopted}$ with its revised uncertainty. After this correction the average precision of our cluster parallaxes is ∼8%.

The Cepheid QZ Nor is a particular case; located at 18 arcmin of NGC 6067, it is a peripherical member of this cluster. The 9σ difference in μ_δ could be explained by the fact that the Cepheid is leaving the cluster. This membership was identified by Anderson et al. (2013) as bona fide. Moreover, QZ Nor is also present in the sample of companions found by Kervella et al. (2019): the stable star *Gaia* DR2 5932565899990412672 is located at 16″ (30 kau) from the Cepheid. Its GDR2 parallax of 0.452 ± 0.130 mas agrees particularly well with the 0.443 ± 0.036 mas parallax of NGC 6067 from Cantat-Gaudin et al. (2018). Therefore, we decided to include this pair.

The cross-match also resulted in potential members that only have 2MASS single epoch photometry available. Since average magnitudes are preferred for the Leavitt law calibration, we discarded these pairs. In that case, we found V379 Cas, GU Nor, and XZ Car to be members of NGC 129, NGC 6067, and NGC 3496 respectively.

A comparison between direct GDR2 Cepheid parallaxes and the corresponding open cluster parallaxes from Cantat-Gaudin et al. (2018) is displayed in Fig. 2. The field charts of each open cluster Cepheid are displayed in Fig. A.1.

2.3. Photometry

In order to determine the phase-averaged magnitudes of the CCs in our sample, we searched them in the catalog assembled by Groenewegen (2018). It is a compilation of mean apparent magnitudes in J, H, K, and V bands in different photometric systems, taken from different sources (see Table 3). Laney & Stobie (1992) provide NIR magnitudes in the SAAO system, to which we set the uncertainties to 0.008 mag following Groenewegen (2018). For homogeneity we converted them into the 2MASS system using the equations from Koen et al. (2007):

$$J_{\rm 2MASS} = -0.028 + J_{\rm SAAO} - 0.047(J_{\rm SAAO} - K_{\rm SAAO}),$$
$$H_{\rm 2MASS} = +0.014 + H_{\rm SAAO},$$
$$K_{\rm 2MASS} = -0.015 + K_{\rm SAAO} + 0.177(H_{\rm SAAO} - K_{\rm SAAO})$$
$$- 0.082(J_{\rm SAAO} - H_{\rm SAAO})^2.$$

The magnitudes given by Monson & Pierce (2011) are in the BIRCAM photometric system, we also adopted uncertainties of 0.008 mag, and the magnitudes taken from Welch et al. (1984) and Barnes et al. (1997) are in the CIT photometric system, with uncertainties of 0.010 mag following Groenewegen (2018). They were all converted into the 2MASS system using the equations from Monson & Pierce (2011):

$$K_{\rm 2MASS} = K_{\rm BIRCAM} + 0.008 (J_{\rm BIRCAM} - K_{\rm BIRCAM}) - 0.042,$$
$$J_{\rm 2MASS} = K_{\rm 2MASS} + 1.052 (J_{\rm BIRCAM} - K_{\rm BIRCAM}) - 0.002,$$
$$H_{\rm 2MASS} = K_{\rm 2MASS} + 0.993 (H_{\rm BIRCAM} - K_{\rm BIRCAM}) + 0.050,$$

Table 3. Final sample adopted, combining Cepheids with resolved companions and open cluster Cepheids.

Cepheid	P (days)	$\varpi^{(*)}$ (mas)	$E(B-V)$	m_V (mag)	m_J (mag)	m_H (mag)	m_{K_S} (mag)	$m_H^{W\,(**)}$ (mag)	Ref$_{NIR}$
Sample of Cepheids with resolved companions									
DF Cas	3.832	$0.367_{\pm0.104}$	$0.564_{\pm0.049}$	$10.880_{\pm0.030}$	$8.488_{\pm0.025}$	$8.036_{\pm0.025}$	$7.879_{\pm0.025}$	$7.533_{\pm0.066}$	G14
CM Sct	3.917	$0.518_{\pm0.056}$	$0.775_{\pm0.045}$	$11.100_{\pm0.030}$	$8.300_{\pm0.025}$	$7.818_{\pm0.025}$	$7.558_{\pm0.025}$	$7.240_{\pm0.066}$	G14
EV Sct	$4.396^{(\star)}$	$0.481_{\pm0.040}$	$0.623_{\pm0.015}$	$10.130_{\pm0.030}$	$7.608_{\pm0.008}$	$7.184_{\pm0.008}$	$7.018_{\pm0.008}$	$6.658_{\pm0.061}$	L92
TV CMa	4.670	$0.426_{\pm0.054}$	$0.574_{\pm0.029}$	$10.590_{\pm0.030}$	$8.022_{\pm0.008}$	$7.582_{\pm0.008}$	$7.364_{\pm0.008}$	$7.048_{\pm0.061}$	M11
V532 Cyg	$4.675^{(\star)}$	$0.619_{\pm0.033}$	$0.519_{\pm0.007}$	$9.090_{\pm0.030}$	$6.863_{\pm0.025}$	$6.393_{\pm0.025}$	$6.250_{\pm0.025}$	$5.919_{\pm0.066}$	2MASS
V950 Sco	$4.814^{(\star)}$	$0.893_{\pm0.069}$	$0.251_{\pm0.019}$	$7.310_{\pm0.030}$	$5.681_{\pm0.008}$	$5.439_{\pm0.008}$	$5.295_{\pm0.008}$	$5.083_{\pm0.061}$	G18
V350 Sgr	5.154	$1.015_{\pm0.048}$	$0.308_{\pm0.008}$	$7.470_{\pm0.030}$	$5.625_{\pm0.010}$	$5.245_{\pm0.010}$	$5.121_{\pm0.010}$	$4.844_{\pm0.061}$	W84
VW Cru	5.265	$0.679_{\pm0.034}$	$0.640_{\pm0.046}$	$9.600_{\pm0.030}$	$6.805_{\pm0.025}$	$6.261_{\pm0.025}$	$6.051_{\pm0.025}$	$5.681_{\pm0.066}$	G14
AX Cir	5.273	$1.725_{\pm0.527}$	$0.265_{\pm0.121}$	$5.880_{\pm0.030}$	$4.299_{\pm0.025}$	$3.879_{\pm0.025}$	$3.780_{\pm0.025}$	$3.524_{\pm0.066}$	G14
δ Cep	5.366	$3.364_{\pm0.049}$	$0.075_{\pm0.018}$	$3.950_{\pm0.030}$	$2.683_{\pm0.010}$	$2.396_{\pm0.010}$	$2.294_{\pm0.010}$	$2.104_{\pm0.061}$	B97
CV Mon	5.379	$0.508_{\pm0.040}$	$0.705_{\pm0.018}$	$10.310_{\pm0.030}$	$7.314_{\pm0.008}$	$6.781_{\pm0.008}$	$6.529_{\pm0.008}$	$6.165_{\pm0.061}$	M11
QZ Nor	$5.401^{(\star)}$	$0.452_{\pm0.132}$	$0.289_{\pm0.020}$	$8.870_{\pm0.030}$	$7.085_{\pm0.008}$	$6.748_{\pm0.008}$	$6.614_{\pm0.008}$	$6.360_{\pm0.061}$	L92
V659 Cen	5.622	$1.355_{\pm0.448}$	$0.151_{\pm0.034}$	$6.620_{\pm0.030}$	$5.177_{\pm0.025}$	$4.907_{\pm0.025}$	$4.651_{\pm0.025}$	$4.583_{\pm0.066}$	G14
CS Vel	5.905	$0.222_{\pm0.050}$	$0.716_{\pm0.027}$	$11.700_{\pm0.030}$	$8.771_{\pm0.008}$	$8.246_{\pm0.008}$	$8.011_{\pm0.008}$	$7.643_{\pm0.061}$	L92
RS Nor	6.198	$0.449_{\pm0.043}$	$0.577_{\pm0.036}$	$10.000_{\pm0.030}$	$7.412_{\pm0.010}$	$6.794_{\pm0.010}$	$6.683_{\pm0.010}$	$6.249_{\pm0.061}$	SPIPS
X Cru	6.220	$0.609_{\pm0.061}$	$0.294_{\pm0.019}$	$8.400_{\pm0.030}$	$6.521_{\pm0.025}$	$6.125_{\pm0.025}$	$5.935_{\pm0.025}$	$5.717_{\pm0.066}$	G14
AW Per	6.464	$1.046_{\pm0.349}$	$0.479_{\pm0.016}$	$7.480_{\pm0.030}$	$5.213_{\pm0.008}$	$4.832_{\pm0.008}$	$4.657_{\pm0.008}$	$4.354_{\pm0.061}$	M11
U Sgr	6.745	$1.461_{\pm0.038}$	$0.408_{\pm0.007}$	$6.690_{\pm0.030}$	$4.506_{\pm0.008}$	$4.100_{\pm0.008}$	$3.912_{\pm0.008}$	$3.637_{\pm0.061}$	M11
ER Car	7.720	$0.889_{\pm0.210}$	$0.111_{\pm0.016}$	$6.820_{\pm0.030}$	$5.310_{\pm0.008}$	$5.034_{\pm0.008}$	$4.896_{\pm0.008}$	$4.698_{\pm0.061}$	G18
SX Vel	9.550	$0.432_{\pm0.086}$	$0.237_{\pm0.014}$	$8.290_{\pm0.030}$	$6.500_{\pm0.008}$	$6.133_{\pm0.008}$	$5.991_{\pm0.008}$	$5.743_{\pm0.061}$	L92
SY Nor	12.646	$0.414_{\pm0.053}$	$0.611_{\pm0.059}$	$9.500_{\pm0.030}$	$6.574_{\pm0.008}$	$6.105_{\pm0.008}$	$5.865_{\pm0.008}$	$5.504_{\pm0.061}$	G18
RS Pup	41.443	$0.503_{\pm0.045}$	$0.451_{\pm0.010}$	$7.010_{\pm0.030}$	$4.365_{\pm0.008}$	$3.828_{\pm0.008}$	$3.619_{\pm0.008}$	$3.276_{\pm0.061}$	L92
Sample of open cluster Cepheids									
CG Cas	4.365	$0.282_{\pm0.041}$	$0.667_{\pm0.009}$	$11.380_{\pm0.030}$	$8.903_{\pm0.025}$	$8.299_{\pm0.025}$	$8.109_{\pm0.025}$	$7.775_{\pm0.066}$	G14
EV Sct	$4.398^{(\star)}$	$0.468_{\pm0.035}$	$0.623_{\pm0.015}$	$10.130_{\pm0.030}$	$7.608_{\pm0.008}$	$7.184_{\pm0.008}$	$7.018_{\pm0.008}$	$6.658_{\pm0.061}$	L92
CF Cas	4.875	$0.269_{\pm0.041}$	$0.556_{\pm0.021}$	$11.060_{\pm0.030}$	$8.590_{\pm0.008}$	$8.126_{\pm0.008}$	$7.900_{\pm0.008}$	$7.608_{\pm0.061}$	M11
CV Mon	5.379	$0.523_{\pm0.043}$	$0.705_{\pm0.018}$	$10.310_{\pm0.030}$	$7.314_{\pm0.008}$	$6.781_{\pm0.008}$	$6.529_{\pm0.008}$	$6.165_{\pm0.061}$	M11
QZ Nor	$5.401^{(\star)}$	$0.443_{\pm0.036}$	$0.289_{\pm0.020}$	$8.870_{\pm0.030}$	$7.085_{\pm0.008}$	$6.748_{\pm0.008}$	$6.614_{\pm0.008}$	$6.360_{\pm0.061}$	L92
V Cen	5.495	$1.288_{\pm0.023}$	$0.265_{\pm0.016}$	$6.820_{\pm0.030}$	$5.019_{\pm0.008}$	$4.642_{\pm0.008}$	$4.498_{\pm0.008}$	$4.249_{\pm0.061}$	L92
CS Vel	5.905	$0.221_{\pm0.042}$	$0.716_{\pm0.027}$	$11.700_{\pm0.030}$	$8.771_{\pm0.008}$	$8.246_{\pm0.008}$	$8.011_{\pm0.008}$	$7.643_{\pm0.061}$	L92
V367 Sct	6.293	$0.467_{\pm0.041}$	$1.145_{\pm0.043}$	$11.610_{\pm0.030}$	$7.605_{\pm0.008}$	$6.955_{\pm0.008}$	$6.651_{\pm0.008}$	$6.152_{\pm0.061}$	L92
U Sgr	6.745	$1.514_{\pm0.024}$	$0.408_{\pm0.007}$	$6.690_{\pm0.030}$	$4.506_{\pm0.008}$	$4.100_{\pm0.008}$	$3.912_{\pm0.008}$	$3.636_{\pm0.061}$	M11
RS Ori	7.567	$0.553_{\pm0.027}$	$0.332_{\pm0.010}$	$8.410_{\pm0.030}$	$6.398_{\pm0.008}$	$6.020_{\pm0.008}$	$5.860_{\pm0.008}$	$5.589_{\pm0.061}$	M11
DL Cas	8.001	$0.511_{\pm0.031}$	$0.487_{\pm0.005}$	$8.970_{\pm0.030}$	$6.550_{\pm0.008}$	$6.101_{\pm0.008}$	$5.892_{\pm0.008}$	$5.593_{\pm0.061}$	M11
S Nor	9.754	$1.025_{\pm0.027}$	$0.182_{\pm0.008}$	$6.420_{\pm0.030}$	$4.674_{\pm0.008}$	$4.288_{\pm0.008}$	$4.149_{\pm0.008}$	$3.905_{\pm0.061}$	L92
TW Nor	10.786	$0.383_{\pm0.042}$	$1.190_{\pm0.023}$	$11.670_{\pm0.030}$	$7.442_{\pm0.008}$	$6.712_{\pm0.008}$	$6.375_{\pm0.008}$	$5.865_{\pm0.061}$	L92
V340 Nor	11.288	$0.443_{\pm0.036}$	$0.312_{\pm0.009}$	$8.370_{\pm0.030}$	$6.211_{\pm0.008}$	$5.745_{\pm0.008}$	$5.573_{\pm0.008}$	$5.284_{\pm0.061}$	L92

Notes. Parallaxes in the first part of the table are from GDR2 for the companions; parallaxes in the second part are from Cantat-Gaudin et al. (2018) based on GDR2 with revised uncertainties. Reddenings $E(B-V)$ are taken from the DDO database (Fernie et al. 1995), to which we applied a multiplicative factor of 0.94. Mean apparent magnitudes in V, J, H, K_S bands are from the catalog compiled by Groenewegen (2018): V band magnitudes are originally from Mel'nik et al. (2015) and NIR magnitudes are converted in the 2MASS system with the original references provided in the last column. Apparent Wesenheit magnitudes on the WFC3 system (m_H^W) are also provided; their uncertainties include the photometric transformation errors. $^{(\star)}$ Cepheid pulsating in the first-overtone mode. In this case the period was converted following the approach described in Sect. 2.4. $^{(*)}$ The parallaxes presented in this table do not include the parallax zero-point offset term. $^{(**)}$ m_H^W apparent magnitudes presented in this table do not include the addition of the CRNL term.

References. (G14) Genovali et al. (2014); (L92) Laney & Stobie (1992); (M11) Monson & Pierce (2011); (2MASS) Skrutskie et al. (2006); (G18) Groenewegen (2018); (W84) Welch et al. (1984); (B97) Barnes et al. (1997); (SPIPS) Light curve fitting with the SPIPS algorithm (Mérand et al. 2015; Trahin 2019).

and

$K_{2MASS} = K_{CIT} + 0.001\,(J_{CIT} - K_{CIT}) - 0.019,$
$J_{2MASS} = K_{2MASS} + 1.068\,(J_{CIT} - K_{CIT}) - 0.020,$
$H_{2MASS} = K_{2MASS} + 1.000\,(H_{CIT} - K_{CIT}) + 0.034.$

The NIR magnitudes from Genovali et al. (2014) are derived by template fitting and provided in the 2MASS system. For the

remaining stars the mean magnitude is computed as the median of the available data in Welch et al. (1984), Schechter et al. (1992), and 2MASS (Skrutskie et al. 2006). For RS Nor, the averaged NIR magnitudes were derived by fitting the photometric light curves using the SPIPS algorithm (Mérand et al. 2015). In the V band, all mean magnitudes are provided in the standard

Johnson system and taken from Mel'nik et al. (2015). An uncertainty of 0.03 mag on those magnitudes is adopted.

Based on apparent magnitudes, we built the reddening-free Wesenheit magnitudes m_H^W (Madore 1982), which are a combination of HST-band apparent magnitudes defined by Riess et al. (2018b) as

$$m_H^W = F160W - R(F555W - F814W), \quad (2)$$

where $R = 0.386$ is derived from the Fitzpatrick (1999) formulation with $R_V = 3.3$.

Different formulations for the extinction law are available in the literature (Savage & Mathis 1979; Cardelli et al. 1989). We adopt the Fitzpatrick (1999) formulation with $R_V = 3.3$, which yields $R_J = 0.86$, $R_H = 0.55$, and $R_K = 0.37$. This allows a direct comparison of our calibration with that of Riess et al. (2016), based on HST Fine Guidance Sensor (FGS) and HST Wide Field Camera 3 (WFC3) measurements (see Sects. 3.2 and 3.3).

Riess et al. (2018a) provides photometric data in the $F160W$, $F555W$, and $F814W$ bands for 50 MW Cepheids. Using the stars in common between this sample and the Groenewegen (2018) catalog, we derive the set of linear transformations between HST system and ground-based apparent magnitudes, with a scatter of 0.06 mag:

$$F160W = H + 0.25(J - H) - 0.030,$$
$$F555W = V + 0.28(J - H) + 0.020,$$
$$F814W = V - 0.47(V - H) - 0.035.$$

We note that the transformation from ground-based magnitudes into the HST system requires accounting for the count-rate non-linearity (CRNL) effect (Riess et al. 2018a). This bias affects the infrared detectors on WFC3, and has the consequence of decreasing the magnitude of faint stars like extragalactic CCs, compared to bright stars like Milky Way CCs. This correction is performed by adding 0.026 mag to HST $F160W$ apparent magnitudes (Riess et al. 2019a).

We account for the width of the instability strip (IS) by adding in quadrature an additional term in the photometry errors listed in Table 3. In the V band, Macri et al. (2006) find a dispersion of 0.23 mag; an intrinsic width of 0.22 mag is obtained after subtracting the estimated measurement errors. In the J and H bands, Madore et al. (2017) find a scatter of 0.12 mag, which leaves an intrinsic width of 0.11 mag in NIR bands. In the K_S band, Persson et al. (2004) find a scatter of 0.084 mag based on a Large Magellanic Cloud (LMC) study, which leaves 0.07 mag for the width of the IS after subtracting error measurements. Finally, Riess et al. (2019b) find a dispersion of 0.075 mag in the W_H band, yielding an intrinsic width of 0.07 mag for the IS.

In order to compute absolute magnitudes, we need to correct apparent magnitudes from interstellar absorption. We take $E(B - V)$ values from the DDO database (Fernie et al. 1995), which is a compilation of various $E(B - V)$ values from the literature determined in the same system. Following Groenewegen (2018), we apply a multiplicative factor of 0.94 to these reddening values.

2.4. Pulsation modes

The identification of first-overtone (FO) Cepheids is essential for the Leavitt law calibration. These stars belong to a parallel sequence on the PL plane and their pulsation period can be converted into a fundamentalized period (Feast & Catchpole 1997; Kovtyukh et al. 2016). We reviewed the different pulsation modes found in the literature for the stars in our sample

Table 4. Pulsation mode of the Cepheids in our sample.

Cepheid	GDR2	Literature	Adopted
AW Per	FU	FU [a,b]	FU
AX Cir	FU	FU [a,b]	FU
BP Cir	FO	FU [b], FO [a,c,d,e]	★
CF Cas	FU	FU [a,b]	FU
CG Cas	FU	FU [a,b]	FU
CM Sct	FU	FU [a,b]	FU
CS Vel	FU	FU [a,b]	FU
CV Mon	–	FU [b]	FU
δ Cep	–	FU [b]	FU
DF Cas	FU	FU [a]	FU
DL Cas	FU	FU [a,b]	FU
DK Vel	FO	FU [b], FO [a,c]	★
ER Car	FU	FU [a,b]	FU
EV Sct	FO	FO [a,b]	FO
QZ Nor	FO	FU [b], FO [a]	FO
RS Nor	FU	FU [a,b]	FU
RS Ori	FO	FU [a,b]	FU
RS Pup	FU	FU [a,b]	FU
S Nor	FU	FU [a,b]	FU
SX Vel	FU	FU [a,b]	FU
SY Nor	FU	FU [a,b]	FU
TV CMa	FU	FU [a,b]	FU
TW Nor	–	FU [b]	FU
U Sgr	FU	FU [a,b]	FU
V340 Nor	–	FU [a,b]	FU
V350 Sgr	FO	FU [a,b]	FU
V367 Sct	–	FU [f], FO [b]	FU
V532 Cyg	FO	FU [b], FO [a]	FO
V659 Cen	FU	FU [b], FO [a,c]	FU
V950 Sco	FO	FU [b], FO [a]	FO
V Cen	FU	FU [a,b]	FU
VW Cru	FU	FU [a,b]	FU
X Cru	FU	FU [a,b]	FU

Notes. FU = fundamental; FO = first overtone; ★ = excluded because of uncertain pulsation mode.
References. (a) Ripepi et al. (2019); (b) Luck (2018); (c) Zabolotskikh et al. (2004); (d) Evans et al. (1992); (e) Usenko et al. (2014); (f) Anderson et al. (2013).

and followed in particular the pulsation modes provided by the reclassification from Ripepi et al. (2019).

The pulsation modes for the Cepheids in our sample are displayed in Table 4. The second and third column of this table give the pulsation mode provided by the GRD2 catalog and by the literature, respectively. The last column gives the adopted pulsation mode.

For BP Cir and DK Vel, different pulsation modes were found: they are both classified as FO Cepheids by GDR2 and other studies (Zabolotskikh et al. 2004; Ripepi et al. 2019), while they are listed as fundamentals by Luck (2018). The two stars are also consistent with fundamental pulsators in the PL plane. Given the disagreement between the different references about the pulsation mode of BP Cir and DK Vel, we decided to exclude them from the sample.

In order to establish accurate PL and PW relations without excluding the first overtones, we converted their observed periods P_{FO} into the fundamental mode equivalent period P_F using

Table 5. Period conversion of first overtones into fundamental pulsators.

Cepheid	$P_{\rm FO}$	$P_{\rm F}$
EV Sct	3.091	4.396
V532 Cyg	3.284	4.675
V950 Sco	3.380	4.814
QZ Nor	3.786	5.401

the equation by Kovtyukh et al. (2016):

$$P_{\rm FO}/P_{\rm F} = -0.0239_{\pm 0.0031} \log P_{\rm F} - 0.0404_{\pm 0.0035} \, [{\rm Fe/H}]$$
$$+ 0.7187_{\pm 0.0017}.$$

Field and cluster Cepheids have similar distributions in the Galactic plane, so they have similar metallicity distributions and both can be assumed close to solar (Romaniello et al. 2008). The first overtones of the sample have periods $P_{\rm FO}$ comprised between 3 and 4 days. In this range of periods, we can approximate the previous equation by the linear relation:

$$P_{\rm F} = 1.4459 \, P_{\rm FO} - 0.0736. \tag{3}$$

The conversion of first overtones into fundamentals is listed in Table 5. The positions of these Cepheids in the PL plane after the transformation are consistent with the distribution of fundamental pulsators.

Even though converting first overtones into fundamentals may introduce a small uncertainty on periods, we decided to include them in the sample for the calibration of the Leavitt law. The periods obtained after conversion with the relations from Feast & Catchpole (1997) and Kovtyukh et al. (2016) only differ by 0.006 days. Gallenne et al. (2018) find a difference of less than 1% between an empirical conversion law and a theoretical one. Including the five first overtones of the sample with their modified periods instead of rejecting them introduces only a very small change on the intercept of the PL relation and improves the precision of the fit.

3. Results

3.1. Calibration of the Leavitt law

In this section we combine the 22 Cepheid companions with the 14 open cluster Cepheids. Their parameters are listed in Table 3. We found five Cepheids present in both samples. For these five stars the companion parallax and the cluster parallax agree within 1σ except for U Sgr, which is at 1.2σ. In order to avoid any correlation between our two sets of parallaxes, for these five stars we recomputed the Cantat-Gaudin et al. (2018) cluster parallaxes as the median of all stars parallaxes after excluding the companion. We found our new cluster parallaxes to differ by $0.5\,\mu{\rm as}$ at most from the original values, so we adopted these new parallax values and considered the two sources of measurement to be independent and non-correlated. For these five Cepheids, both parallax measurements (cluster and companion) are considered independently in the linear fit.

In order to calibrate the PL relations and the Period–Wesenheit (PW) relations, we used the approach introduced by Feast & Catchpole (1997) and Arenou et al. (1999) and we computed the Astrometric Based Luminosity (ABL), defined as

$$ABL = 10^{0.2 M_\lambda} = \varpi \, 10^{0.2 m_\lambda - 2}, \tag{4}$$

where M_λ is the absolute magnitude, m_λ is the dereddened apparent magnitude, and ϖ is the parallax in milliarcseconds. Cali-
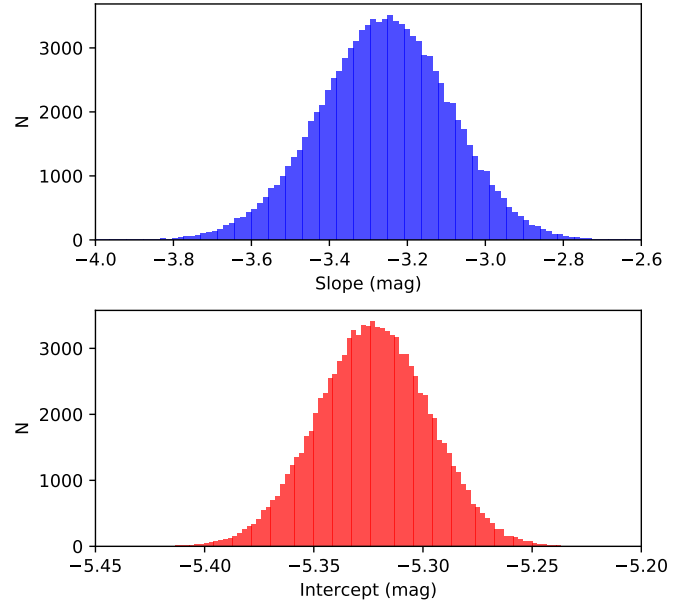

Fig. 3. Results of the Monte Carlo technique for a PL fit of the form $K_S = a(\log P - \log P_0) + b$ where $\log P_0 = 0.84$. *Top and bottom panels*: distribution of the slope a and intercept b, respectively.

brating the Leavitt Law following this approach is equivalent to determining the coefficients a and b in the equation

$$ABL = 10^{0.2 \, [a(\log P - \log P_0) + b]}. \tag{5}$$

We performed a weighted fit of the ABL function by using the `curve_fit` function from the python Scipy library. The robustness of the fit and of the uncertainties is ensured by a Monte Carlo approach, applied with 100 000 iterations. The distributions of the slope and zero-point of our K_S Leavitt law obtained by this technique are displayed via histograms in Fig. 3.

We used the formalism detailed in Gallenne et al. (2017), i.e., we adopted the linear parameterization

$$M_\lambda = b_\lambda + a_\lambda \, (\log P - \log P_0), \tag{6}$$

where a_λ and b_λ are respectively the slope and the zero-point of the PL relation. This parameterization removes the correlation between a_λ and b_λ and minimizes their respective uncertainties. The optimum value of $\log P_0$ depends on the dataset (see Gallenne et al. (2017) for further details)

$$\log P_0 = \frac{\langle \log P_i / e_i^2 \rangle}{\langle 1/e_i^2 \rangle}, \tag{7}$$

where $\log P_i$ are the periods of the stars, and e_i are the uncertainties on their parallax; $\langle \rangle$ denotes the averaging operator. We find our sample centered around $\log P_0 = 0.84$.

GDR2 parallaxes are subject to a zero-point (ZP) off-set, whose value was studied extensively but is still debated. Lindegren et al. (2018) used quasars ($G \sim 19\,{\rm mag}$) to derive that *Gaia* parallaxes are underestimated by 0.029 mas. Arenou et al. (2018) finds a zero-point of -0.0319 mas based on Milky Way Cepheids ($G \sim 8\,{\rm mag}$), in agreement with the -0.031 mas estimate by Graczyk et al. (2019) from detached eclipsing binaries ($G \sim 9\,{\rm mag}$) and surface brightness-color relations. Larger values were also found by Ripepi et al. (2019) and Stassun & Torres (2018), who find zero-point offsets of -0.070 mas and -0.082 mas respectively. Intermediary values were derived by

Table 6. Zero-point offset for GDR2 parallaxes found in the literature.

$\mathrm{ZP_{GDR2}}$ (mas)	Reference	Type of sources	Typical G (mag)
-0.029	Lindegren et al. (2018)	Quasars	19
$-0.031_{\pm0.011}$	Graczyk et al. (2019)	Eclipsing binaries	9
$-0.0319_{\pm0.0008}$	Arenou et al. (2018)	MW Cepheids	8
$-0.035_{\pm0.016}$	Sahlholdt & Silva Aguirre (2018)	Dwarf stars	9
$-0.041_{\pm0.010}$	Hall et al. (2019)	Red giants	13
$-0.046_{\pm0.013}$	Riess et al. (2018a)	MW Cepheids	9
$-0.049_{\pm0.018}$	Groenewegen (2018)	MW Cepheids (HST)	8
$-0.053_{\pm0.003}$	Zinn et al. (2019)	Red giants	13
$-0.054_{\pm0.006}$	Schönrich et al. (2019)	GDR2 RV	12
$-0.057_{\pm0.003}$	Muraveva et al. (2018)	RR Lyrae	12
$-0.070_{\pm0.010}$	Ripepi et al. (2019)	LMC Cepheids	15
$-0.082_{\pm0.033}$	Stassun & Torres (2018)	Eclipsing binaries	9

Table 7. Coefficients of the PL relation obtained with GDR2 parallaxes of companions and open clusters (left) and with direct parallaxes of Cepheids (right), for different parallax zero-point offsets.

Band	a	b	ρ	χ_r^2	σ	a	b	ρ	χ_r^2	σ	ZP (mas)
	Parallaxes of companions and open clusters					Parallaxes of Cepheids					
V	$-2.486_{\pm0.246}$	$-3.782_{\pm0.051}$	0.15	0.27	0.18	$-2.093_{\pm0.236}$	$-3.888_{\pm0.050}$	0.09	0.58	0.23	-0.031
J	$-3.079_{\pm0.187}$	$-4.964_{\pm0.032}$	0.21	0.38	0.16	$-2.680_{\pm0.154}$	$-5.040_{\pm0.033}$	0.03	0.97	0.21	-0.031
H	$-3.223_{\pm0.185}$	$-5.263_{\pm0.032}$	0.21	0.34	0.16	$-2.799_{\pm0.151}$	$-5.331_{\pm0.033}$	0.02	0.91	0.21	-0.031
K_S	$-3.268_{\pm0.165}$	$-5.363_{\pm0.026}$	0.25	0.38	0.14	$-2.856_{\pm0.127}$	$-5.419_{\pm0.028}$	0.01	1.18	0.22	-0.031
W_H	$-3.340_{\pm0.180}$	$-5.476_{\pm0.030}$	0.23	0.41	0.16	$-2.911_{\pm0.141}$	$-5.534_{\pm0.031}$	0.01	0.93	0.20	-0.031
V	$-2.481_{\pm0.244}$	$-3.731_{\pm0.050}$	0.15	0.29	0.18	$-2.111_{\pm0.236}$	$-3.829_{\pm0.050}$	0.09	0.53	0.21	-0.046
J	$-3.068_{\pm0.184}$	$-4.918_{\pm0.032}$	0.21	0.43	0.16	$-2.692_{\pm0.153}$	$-4.987_{\pm0.033}$	0.03	0.90	0.19	-0.046
H	$-3.215_{\pm0.185}$	$-5.217_{\pm0.031}$	0.22	0.37	0.16	$-2.811_{\pm0.151}$	$-5.278_{\pm0.033}$	0.03	0.82	0.19	-0.046
K_S	$-3.257_{\pm0.163}$	$-5.323_{\pm0.026}$	0.25	0.44	0.14	$-2.865_{\pm0.126}$	$-5.370_{\pm0.028}$	0.01	1.09	0.19	-0.046
W_H	$-3.332_{\pm0.177}$	$-5.432_{\pm0.029}$	0.23	0.47	0.17	$-2.923_{\pm0.141}$	$-5.483_{\pm0.031}$	0.01	0.85	0.18	-0.046
V	$-2.475_{\pm0.243}$	$-3.680_{\pm0.050}$	0.15	0.32	0.19	$-2.130_{\pm0.235}$	$-3.771_{\pm0.049}$	0.10	0.50	0.21	-0.061
J	$-3.060_{\pm0.179}$	$-4.874_{\pm0.032}$	0.20	0.52	0.17	$-2.703_{\pm0.153}$	$-4.936_{\pm0.032}$	0.03	0.86	0.18	-0.061
H	$-3.207_{\pm0.183}$	$-5.172_{\pm0.031}$	0.21	0.44	0.17	$-2.824_{\pm0.151}$	$-5.226_{\pm0.032}$	0.03	0.76	0.17	-0.061
K_S	$-3.248_{\pm0.162}$	$-5.283_{\pm0.025}$	0.24	0.55	0.16	$-2.873_{\pm0.125}$	$-5.321_{\pm0.027}$	0.01	1.04	0.18	-0.061
W_H	$-3.322_{\pm0.175}$	$-5.389_{\pm0.029}$	0.22	0.58	0.18	$-2.934_{\pm0.140}$	$-5.433_{\pm0.030}$	0.02	0.81	0.17	-0.061

Notes. The equations are of the form $M = a\,(\log P - 0.84) + b$, and ρ is the correlation between a and b.

Riess et al. (2018a) and Groenewegen (2018), who estimate -0.046 mas and -0.049 mas respectively. The recent determinations of $\mathrm{ZP_{GDR2}}$ are listed in Table 6. In the following, we adopt $\mathrm{ZP_{GDR2}} = -0.046$ mas (Riess et al. 2018a) from Cepheids, which is close to the median of all values (see Table 6).

The PL coefficients obtained in different bands are listed in Table 7 for different $\mathrm{ZP_{GDR2}}$ values. The Leavitt law calibration in the K_S band is displayed in Fig. 4. The lower panel shows residuals in terms of parallax, computed as the difference between the input parallax and the parallax given by the best fit. This calibration gives a reduced χ^2 of 0.44 and a dispersion of $\sigma = 0.14$ mag.

An equivalent calibration, based this time on direct Cepheid parallaxes, is presented in Fig. 5. When the CC parallaxes are adopted, we obtain $\chi_r^2 = 1.09$ and a dispersion of $\sigma = 0.19$ mag. The dispersion of the PL relation based on Cepheid parallaxes (Fig. 5) does not appear to be systematic, but rather results in a larger spread not accounted for in the uncertainties. The PL coefficients derived from GDR2 parallaxes of Cepheids are also provided in Table 7.

We note that very accurate distance measurements are available for a few classical Cepheids, independently of *Gaia* DR2. They can be used to check the consistency of GDR2 parallaxes. The Cepheid RS Pup has been studied in detail by Kervella et al. (2014) who estimated its parallax to 0.524 ± 0.022 mas using polarimetric HST images of the light echoes propagating in its circumstellar nebula (see also Kervella et al. 2017). A second interesting measurement is the distance of the short-period binary Cepheid V1334 Cyg by Gallenne et al. (2018). It is the most precise parallax determination for a Cepheid, with a value of 1.388 ± 0.015 mas. This measurement was obtained by observing the orbit of the system by spectroscopy and optical interferometry. This estimate differs by 3.6σ with the GDR2 parallax value (1.151 ± 0.066 mas). These two independent distance measurements are represented by yellow squares on the PL relations in Figs. 4 and 5, but are not included in the fit since they are not from GDR2. In the case where companion parallaxes and cluster parallaxes are adopted, the two points based on independent measurements agree with the fitted relation at 1σ. However, in the case of a PL relation based on direct Cepheid parallaxes, both
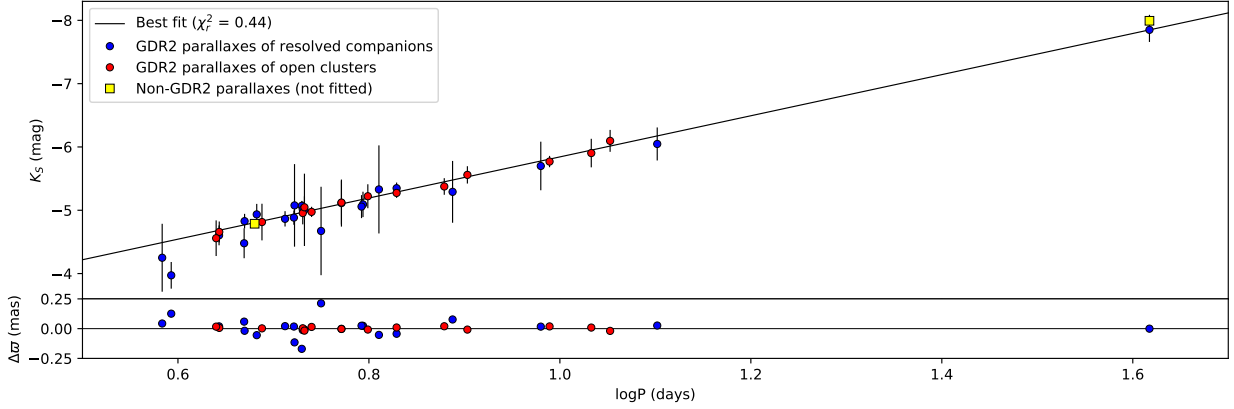
Fig. 4. Period–luminosity diagram in the K_S band calibrated with GDR2 parallaxes of Cepheids companions (blue) and open clusters (red). The two yellow squares are V1334 Cyg and RS Pup; they are not included in the fit of the PL relation.
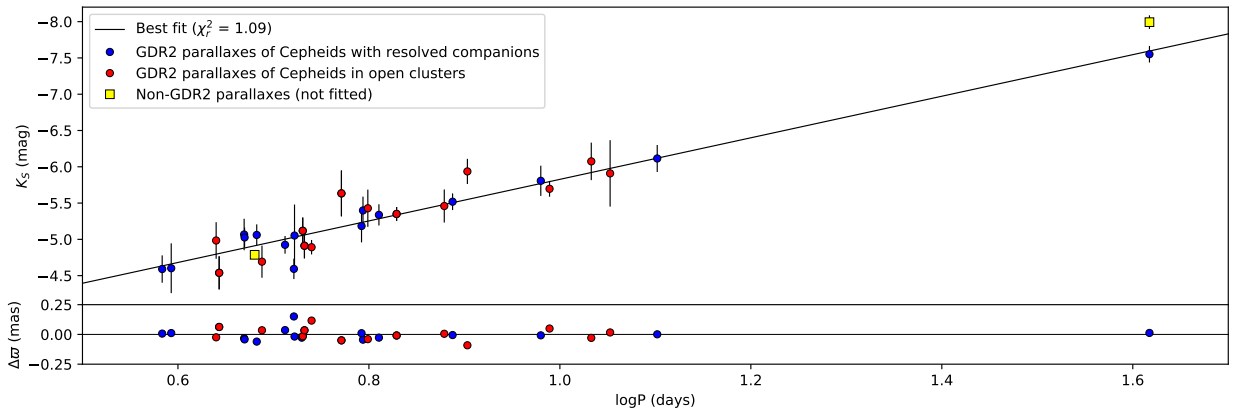

Fig. 5. Same as Fig. 4, but using directly GDR2 parallaxes of Cepheids.

absolute magnitudes derived from the independent points differ by 2.9σ from the best fit. The Cepheid RS Pup is particularly interesting since it has a resolved companion listed in our sample (see Table 1). We note that the RS Pup independent estimate is in very good agreement with the GDR2 parallax of RS Pup companion (0.503 ± 0.045 mas), but differs by 0.060 mas from the GDR2 parallax of the Cepheid itself (0.584 ± 0.026 mas).

3.2. Comparison with the literature

In this section, we compare our sample of GDR2 parallaxes with the corresponding parallaxes predicted by a PL calibration based on non-*Gaia* data. Riess et al. (2016; hereafter R16) use ten MW Cepheid parallaxes from HST/FGS (Benedict et al. 2007), three HIPPARCOS measurements and two Cepheids with parallaxes measured by spatial scanning with the HST/WFC3 (Riess et al. 2014; Casertano et al. 2016). These measurements constitute the MW anchor from R16. They combine it with megamasers in NGC 4258 and eight detached eclipsing binaries in the LMC to derive a final Hubble constant $H_0 = 73.24 \pm 1.74$ km s^{-1} Mpc^{-1}, associated with the corresponding PL relation in the Wesenheit HST/WFC3 system:

$$M_H^W = -5.93 - 3.26\,(\log P - 1). \tag{8}$$

For the MW anchor only, the H_0 value is 76.18 ± 2.37 km s^{-1} Mpc^{-1}. From the ratio of the two H_0 values, we offset Eq. (8) and derive the following PL relation for MW Cepheids only:

$$M_H^W = -5.85 - 3.26\,(\log P - 1). \tag{9}$$

We use this Galactic PL calibration based on the Milky Way anchor to compute the predicted parallaxes ϖ_{R16} for each star in our sample:

$$5 \log \varpi_{R16} = M_H^W - m_H^W + 10. \tag{10}$$

Here m_H^W is the apparent magnitude in the Wesenheit system corrected for the CRNL effect (see Sect. 2.3) and M_H^W is derived from the PL relation given by Eq. (9).

The choice of an R value in agreement with Riess et al. (2016) (see Sect. 3) ensures the consistency of this comparison. To account for the width of the instability strip ($\sigma = 0.07$ mag in the W_H band) and for the photometric transformations from ground to HST system ($\sigma = 0.06$ mag), we set the apparent magnitudes uncertainties to 0.09 mag. Figure 6 shows the comparison between the GDR2 parallaxes of our sample of stars corrected by a -0.046 mas offset and the predicted parallaxes from R16. The GDR2 parallaxes appear to be slightly underestimated compared with the predicted values, especially for Cepheids with large parallax values.

The prototype δ Cep is particularly interesting for this study: it hosts a resolved companion with a GDR2 parallax and it is also present in the sample of HST/FGS parallaxes by Benedict et al. (2007). The GDR2 parallax of its companion is 3.393 ± 0.049 mas, while its HST/FGS parallax is 3.66 ± 0.15 mas. These two measurements differ by 1.7σ (7% in relative terms), which agrees with the general trend observed in Fig. 6. We note that δ Cep has no valid parallax in GDR2, so its companion parallax is the only possible alternative to HST/FGS measurements.
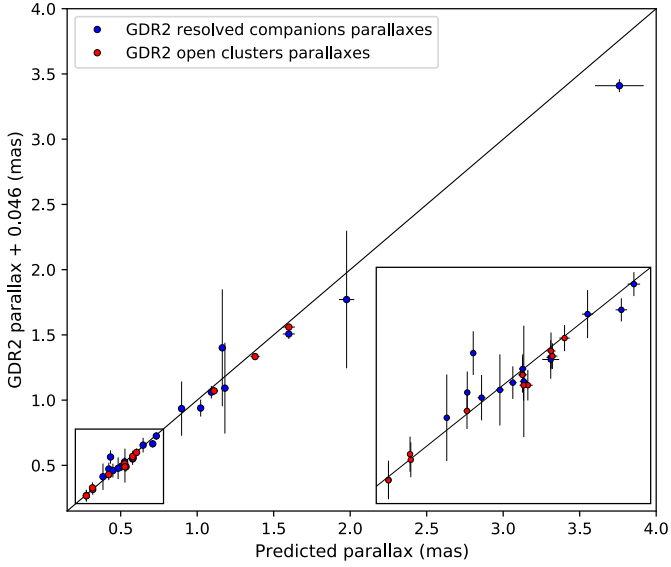
Fig. 6. Comparison of GDR2 parallaxes of resolved companions and open clusters hosting Cepheids with the predicted parallaxes using the MW PL calibration given in Eq. (9). The solid black line corresponds to the identity line.

In Table 8 we present different PL calibrations found in the literature based on various methods and data. Benedict et al. (2007) derive a K-band PL relation based on HST/FGS parallaxes of seven Galactic Cepheids in the CIT system. We converted this result in the 2MASS system using the relation from Carpenter (2001). The investigation by Fouqué et al. (2007) provides a PL calibration in the K_S band, based on HST/FGS and HIPPARCOS parallaxes, as well as infrared surface brightness (IRSB) and interferometric Baade-Wesselink parallaxes. Recently, Gieren et al. (2018) derived a calibration of the PL relation using a IRSB Baade-Wesselink-type method to determine individual distances to the Cepheids. The result is in the UKIRT system, but the transformation between UKIRT and 2MASS systems given in Carpenter (2001) shows that this transformation can be neglected. Finally, Groenewegen (2018) established a K_S-band PL relation based on a large sample of Cepheids parallaxes from GDR2. In Table 8, we report the coefficients obtained after adopting a GDR2 parallax zero-point of -0.046 mas.

We note that our intercept is very similar to that found by Groenewegen (2018), also based on GDR2 data. However, our calibration shows a significant difference (~ 0.1–0.2 mag) in intercept with previous calibrations based on HST/FGS data (Benedict et al. 2007; Fouqué et al. 2007).

3.3. Implications on the distance scale

The determination of the Hubble constant by Planck Collaboration VI (2020) exhibit a tension at the $\sim 5\sigma$ level with the latest empirical estimate by Riess et al. (2019b) based on LMC Cepheids combined with masers in NGC 4258 and Milky Way parallaxes measured by the HST/FGS, HST/WFC3, and HIPPARCOS.

Following the method presented in Sect. 4 in Riess et al. (2018b), we translate our previous parallax comparison (see Sect. 3.2) into a comparison in terms of the Hubble constant. We examine the impact of changing the MW anchor alone on the H_0 measurement that depends on three anchors. Therefore, we look at the H_0 value from R16 that pertains only to the MW. We use the relation $H_{0,\text{GDR2}} = \alpha H_{0,\text{R16}}$, where $\alpha = \varpi_{\text{GDR2}}/\varpi_{\text{R16}}$ and $H_{0,\text{R16}}$ is the value anchored to Milky Way Cepheids only and

Table 8. Comparison of our results with other PL relations from the literature.

Reference	α	β
Benedict et al. (2007)	$-3.32_{\pm 0.12}$	$-5.73_{\pm 0.03}$
Fouqué et al. (2007)	$-3.365_{\pm 0.063}$	$-5.647_{\pm 0.066}$
Gieren et al. (2018)	$-3.258_{\pm 0.092}$	$-5.682_{\pm 0.034}$
Groenewegen (2018)	$-3.028_{\pm 0.067}$	$-5.867_{\pm 0.087}$
Present work	$-3.257_{\pm 0.163}$	$-5.844_{\pm 0.037}$

Notes. All equations are expressed in the form $K_S = \alpha(\log P - 1) + \beta$ in the 2MASS system.

Table 9. Hubble constant value derived from the comparison between our GDR2 parallax samples and the predicted parallaxes from R16.

	H_0 (km s^{-1} Mpc^{-1})	H_0 (km s^{-1} Mpc^{-1})
	FU only	FU + FO
Companions	$72.83 \pm 2.10 \pm 1.89$	$72.49 \pm 2.01 \pm 1.88$
Clusters	$73.11 \pm 2.01 \pm 1.90$	$73.00 \pm 1.99 \pm 1.90$
All Cepheids	$72.99 \pm 1.89 \pm 1.90$	$72.76 \pm 1.86 \pm 1.89$

Notes. The first uncertainties are the statistics combined with the systematics, and the second values account for the effect of the GDR2 parallax zero-point. FU = fundamental mode Cepheids; FO = first-overtone mode Cepheids with fundamentalized period.

is equal to $76.18 \pm 2.37\,\text{km s}^{-1}\,\text{Mpc}^{-1}$. The expected parallaxes ϖ_{R16} are derived from Eqs. (9) and (10).

For each star of the sample, we derive the corresponding α value and we adopt a Monte Carlo approach to estimate the final α value averaged over the sample. We performed this calculation on different subsamples and listed the resulting H_0 values in Table 9. The uncertainties on H_0 include the final error on the R16 estimate excluding the anchors (1.8%), the error on the estimation of α, and finally the uncertainties on the photometric relations to convert ground-based magnitudes into HST magnitudes (1.5%). Changing the GDR2 parallax offset by 0.015 mas results in a change of 2.6% in the Hubble constant; therefore, we adopted a confidence interval of 0.015 mas around the -0.046 mas zero-point and added a 2.6% uncertainty to account for this effect.

We obtain a final value of $72.99 \pm 2.68\,\text{km s}^{-1}\,\text{Mpc}^{-1}$ for fundamental modes only, and $72.76 \pm 2.65\,\text{km s}^{-1}\,\text{Mpc}^{-1}$ for all stars included. Both values are very consistent with the LMC and NGC 4258 anchor results derived by Riess et al. (2019b), and also very close to the result by Reid et al. (2019). The last value agrees at the 1σ level with that of Freedman et al. (2020) and at the 2σ level with the Planck Collaboration VI (2020) measurement.

We note that the CCs used to calibrate the PL relation and H_0 have lower mean periods than most extragalactic Cepheids found by HST. Though there is no evidence of a break in the PL relation at $\log P = 1$ for the Wesenheit magnitude system (Bono et al. 1999, 2008; Riess et al. 2016), it remains important to add longer period Cepheids to the parallax calibration to maintain low systematics.

4. Conclusions

We presented an original calibration of the Milky Way Leavitt law based on GDR2 parallaxes of resolved Cepheid companions and on GDR2 parallaxes of open clusters hosting Cepheids.

Companion and cluster members are not subject to large amplitude photometric and color variability, which reduces the potential for systematic parallax uncertainties. The comparison of our calibration with previous works based on non-*Gaia* parallaxes indicates a systematic offset between the two measurements. By replacing the trigonometric parallaxes used in R16 by companion and cluster average parallaxes, we render the Milky Way, the LMC, and NGC 4258 Leavitt Laws more consistent with one another: we find a MW estimate of $73.0 \pm 2.7\,\mathrm{km\,s^{-1}\,Mpc^{-1}}$ for fundamental modes only and of $H_0 = 72.8 \pm 2.7\,\mathrm{km\,s^{-1}\,Mpc^{-1}}$ for all stars included.

The inclusion of the variability of CCs is not expected in the astrometric processing of the third *Gaia* data release. However, the effects of the systematics due to the absence of chromaticity correction on Cepheids parallaxes should be reduced in the next releases thanks to the larger number of measurements. The future developments will help to pursue the community goal to measure H_0 with utmost precision and accuracy.

References

An, D., Terndrup, D. M., & Pinsonneault, M. H. 2007, ApJ, 671, 1640
Anderson, R. I. 2018, A&A, 611, L7
Anderson, R. I., Eyer, L., & Mowlavi, N. 2013, MNRAS, 434, 2238
Anderson, R. I., Saio, H., Ekström, S., Georgy, C., & Meynet, G. 2016, A&A, 591, A8
Arenou, F., & Luri, X. 1999, ASP Conf. Ser., 167, 13
Arenou, F., Luri, X., Babusiaux, C., et al. 2018, A&A, 616, A17
Astropy Collaboration (Price-Whelan, A. M., et al.) 2018, AJ, 156, 123
Barnes, T. G., III, Fernley, J. A., Frueh, M. L., et al. 1997, PASP, 109, 645
Benedict, G. F., McArthur, B. E., Feast, M. W., et al. 2007, AJ, 133, 1810
Bond, H. E., Nelan, E. P., Remage Evans, N., Schaefer, G. H., & Harmer, D. 2018, ApJ, 853, 55
Bono, G., Caputo, F., Castellani, V., & Marconi, M. 1999, ApJ, 512, 711
Bono, G., Caputo, F., Fiorentino, G., Marconi, M., & Musella, I. 2008, ApJ, 684, 102
Cantat-Gaudin, T., Jordi, C., Vallenari, A., et al. 2018, A&A, 618, A93
Cardelli, J. A., Clayton, G. C., & Mathis, J. S. 1989, ApJ, 345, 245
Carpenter, J. M. 2001, AJ, 121, 2851
Casertano, S., Riess, A. G., Anderson, J., et al. 2016, ApJ, 825, 11
Chen, X., de Grijs, R., & Deng, L. 2015, MNRAS, 446, 1268
Clark, J. S., Negueruela, I., Lohr, M. E., et al. 2015, A&A, 584, L12
Clementini, G., Ripepi, V., Molinaro, R., et al. 2019, A&A, 622, A60
Drimmel, R., Bucciarelli, B., & Inno, L. 2019, Res. Notes Am. Astron. Soc., 3, 79
Evans, N. R., Arellano Ferro, A., & Udalska, J. 1992, AJ, 103, 1638
Feast, M. W., & Catchpole, R. M. 1997, MNRAS, 286, L1
Fernie, J. D., Evans, N. R., Beattie, B., & Seager, S. 1995, Inf. Bull. Variable Stars, 4148
Fitzpatrick, E. L. 1999, PASP, 111, 63
Fouqué, P., Arriagada, P., Storm, J., et al. 2007, A&A, 476, 73
Freedman, W. L., Madore, B. F., Hoyt, T., et al. 2020, ApJ, 891, 57
Gaia Collaboration (Brown, A. G. A., et al.) 2018, A&A, 616, A1
Gaia Collaboration (Clementini, G., et al.) 2017, A&A, 605, A79
Gallenne, A., Kervella, P., Mérand, A., et al. 2017, A&A, 608, A18
Gallenne, A., Kervella, P., Evans, N. R., et al. 2018, ApJ, 867, 121
Genovali, K., Lemasle, B., Bono, G., et al. 2014, A&A, 566, A37
Gieren, W., Storm, J., Konorski, P., et al. 2018, A&A, 620, A99
Graczyk, D., Pietrzyński, G., Gieren, W., et al. 2019, ApJ, 872, 85
Groenewegen, M. A. T. 2018, A&A, 619, A8
Hall, O. J., Davies, G. R., Elsworth, Y. P., et al. 2019, MNRAS, 1036
Kervella, P., Bond, H. E., Cracraft, M., et al. 2014, A&A, 572, A7
Kervella, P., Trahin, B., Bond, H. E., et al. 2017, A&A, 600, A127
Kervella, P., Gallenne, A., Evans, N. R., et al. 2019, A&A, 623, A117
Kharchenko, N. V., Piskunov, A. E., Roeser, S., Schilbach, E., & Scholz, R. D. 2013, VizieR Online Data Catalog: J/A+A/558/A53
Koen, C., Marang, F., Kilkenny, D., & Jacobs, C. 2007, MNRAS, 380, 1433
Kovtyukh, V., Lemasle, B., Chekhonadskikh, F., et al. 2016, MNRAS, 460, 2077
Laney, C. D., & Stobie, R. S. 1992, A&AS, 93, 93
Leavitt, H. S. 1908, Ann. Harvard College Observatory, 60, 87
Leavitt, H. S., & Pickering, E. C. 1912, Harvard College Obs. Circular, 173, 1
Lindegren, L. 2018a, Re-normalising the astrometric chi-square in Gaia DR2, Tech. Rep. GAIA-C3-TN-LU-LL-124 (Lund Observatory)
Lindegren, L. 2018b, Gaia DR2 Astrometry
Lindegren, L. 2020, A&A, 633, A1
Lindegren, L., Hernández, J., Bombrun, A., et al. 2018, A&A, 616, A2
Lohr, M. E., Negueruela, I., Tabernero, H. M., et al. 2018, MNRAS, 478, 3825
Luck, R. E. 2018, AJ, 156, 171
Macri, L. M., Stanek, K. Z., Bersier, D., Greenhill, L. J., & Reid, M. J. 2006, ApJ, 652, 1133
Madore, B. F. 1982, ApJ, 253, 575
Madore, B. F., Freedman, W. L., & Moak, S. 2017, ApJ, 842, 42
Majaess, D., Turner, D., Moni Bidin, C., et al. 2011, ApJ, 741, L27
Mel'nik, A. M., Rautiainen, P., Berdnikov, L. N., Dambis, A. K., & Rastorguev, A. S. 2015, Astron. Nachr., 336, 70
Mérand, A., Kervella, P., Breitfelder, J., et al. 2015, A&A, 584, A80
Monson, A. J., & Pierce, M. J. 2011, ApJS, 193, 12
Muraveva, T., Delgado, H. E., Clementini, G., Sarro, L. M., & Garofalo, A. 2018, MNRAS, 481, 1195
Persson, S. E., Madore, B. F., Krzemiński, W., et al. 2004, AJ, 128, 2239
Planck Collaboration VI. 2020, A&A, 641, A6
Proxauf, B., da Silva, R., Kovtyukh, V. V., et al. 2018, A&A, 616, A82
Reid, M. J., Pesce, D. W., & Riess, A. G. 2019, ApJ, 886, L27
Riess, A. G. 2019, Nat. Rev. Phys., 2, 10
Riess, A. G., Casertano, S., Anderson, J., MacKenty, J., & Filippenko, A. V. 2014, ApJ, 785, 161
Riess, A. G., Macri, L. M., Hoffmann, S. L., et al. 2016, ApJ, 826, 56
Riess, A. G., Casertano, S., Yuan, W., et al. 2018a, ApJ, 861, 126
Riess, A. G., Casertano, S., Yuan, W., et al. 2018b, ApJ, 855, 136
Riess, A. G., Narayan, G., & Calamida, A. 2019a, Calibration of the WFC3-IR Count-rate Nonlinearity, Sub-percent Accuracy for a Factor of a Million in Flux, Tech. Rep. (Baltimore: Space Telescope Science Institute)
Riess, A. G., Casertano, S., Yuan, W., Macri, L. M., & Scolnic, D. 2019b, ApJ, 876, 85
Ripepi, V., Molinaro, R., Musella, I., et al. 2019, A&A, 625, A14
Romaniello, M., Primas, F., Mottini, M., et al. 2008, A&A, 488, 731
Sahlholdt, C. L., & Silva Aguirre, V. 2018, MNRAS, 481, L125
Savage, B. D., & Mathis, J. S. 1979, ARA&A, 17, 73
Schechter, P. L., Avruch, I. M., Caldwell, J. A. R., & Keane, M. J. 1992, AJ, 104, 1930
Schönrich, R., McMillan, P., & Eyer, L. 2019, MNRAS, 487, 3568
Skrutskie, M. F., Cutri, R. M., Stiening, R., et al. 2006, AJ, 131, 1163
Stassun, K. G., & Torres, G. 2018, ApJ, 862, 61
Trahin, B. 2019, Theses, Paris Sciences et Lettres; Observatoire de Paris – LESIA ; CNRS
Turner, D. G. 1982, PASP, 94, 1003
Turner, D. G. 1986, AJ, 92, 111
Turner, D. G. 2010, Ap&SS, 326, 219
Turner, D. G., Pedreros, M. H., & Walker, A. R. 1998, AJ, 115, 1958
Usenko, I. A., Kniazev, A. Y., Berdnikov, L. N., & Kravtsov, V. V. 2014, Astron. Lett., 40, 800
Verde, L., Treu, T., & Riess, A. G. 2019, Nat. Astron., 3, 891
Welch, D. L., Wieland, F., McAlary, C. W., et al. 1984, ApJS, 54, 547
Zabolotskikh, M. V., Rastorguev, A. S., & Egorov, I. E. 2004, ASP Conf. Ser., 316, 209
Zinn, J. C., Pinsonneault, M. H., Huber, D., & Stello, D. 2019, ApJ, 878, 136
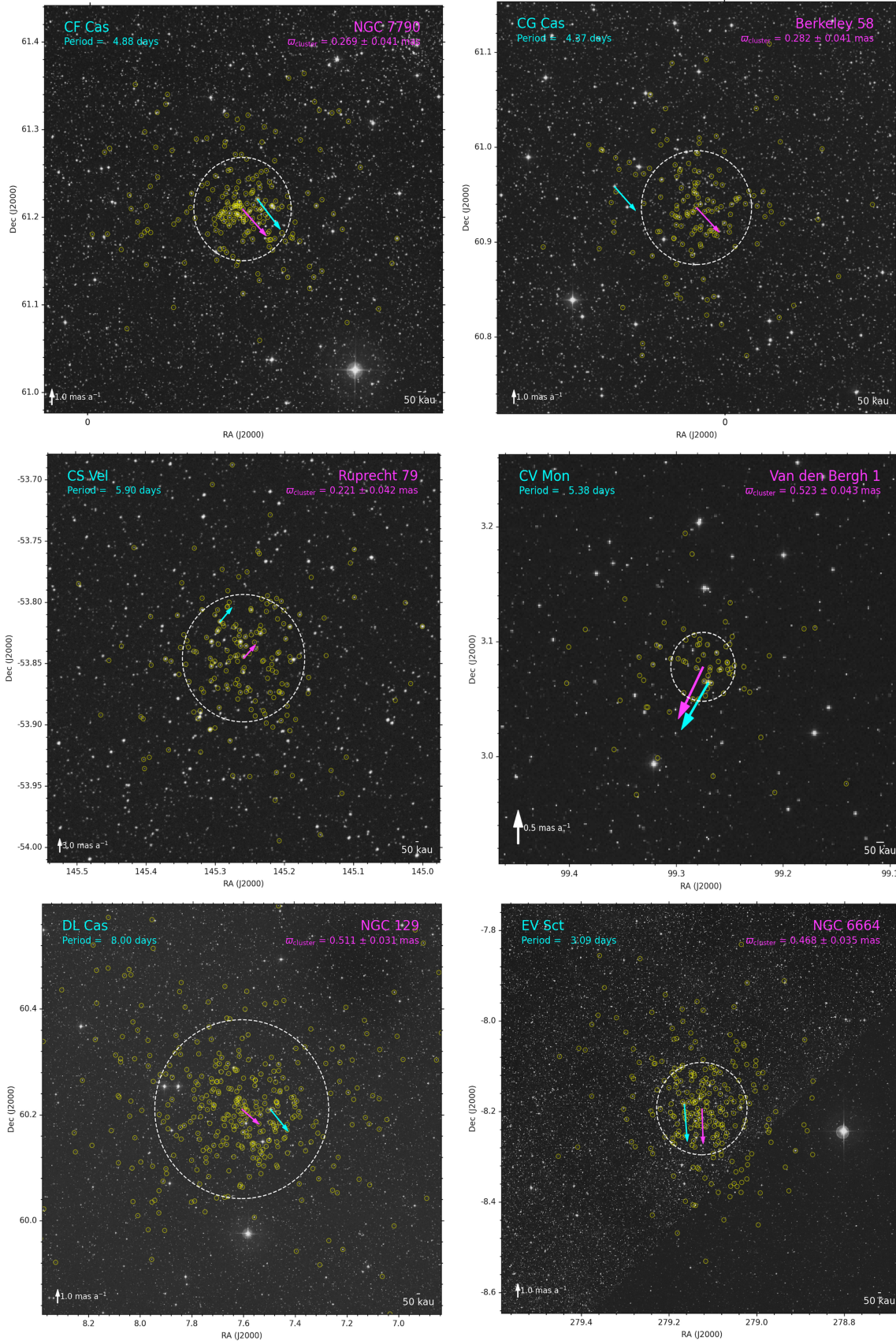
Appendix A: Field charts of open clusters

Fig. A.1. Field charts of our candidate Cepheids in their host clusters. The white dashed circles show the radius r_{50} containing half of the cluster stars, and each yellow circle shows a cluster member. The blue and pink arrows show the Cepheid and cluster proper motion, respectively.
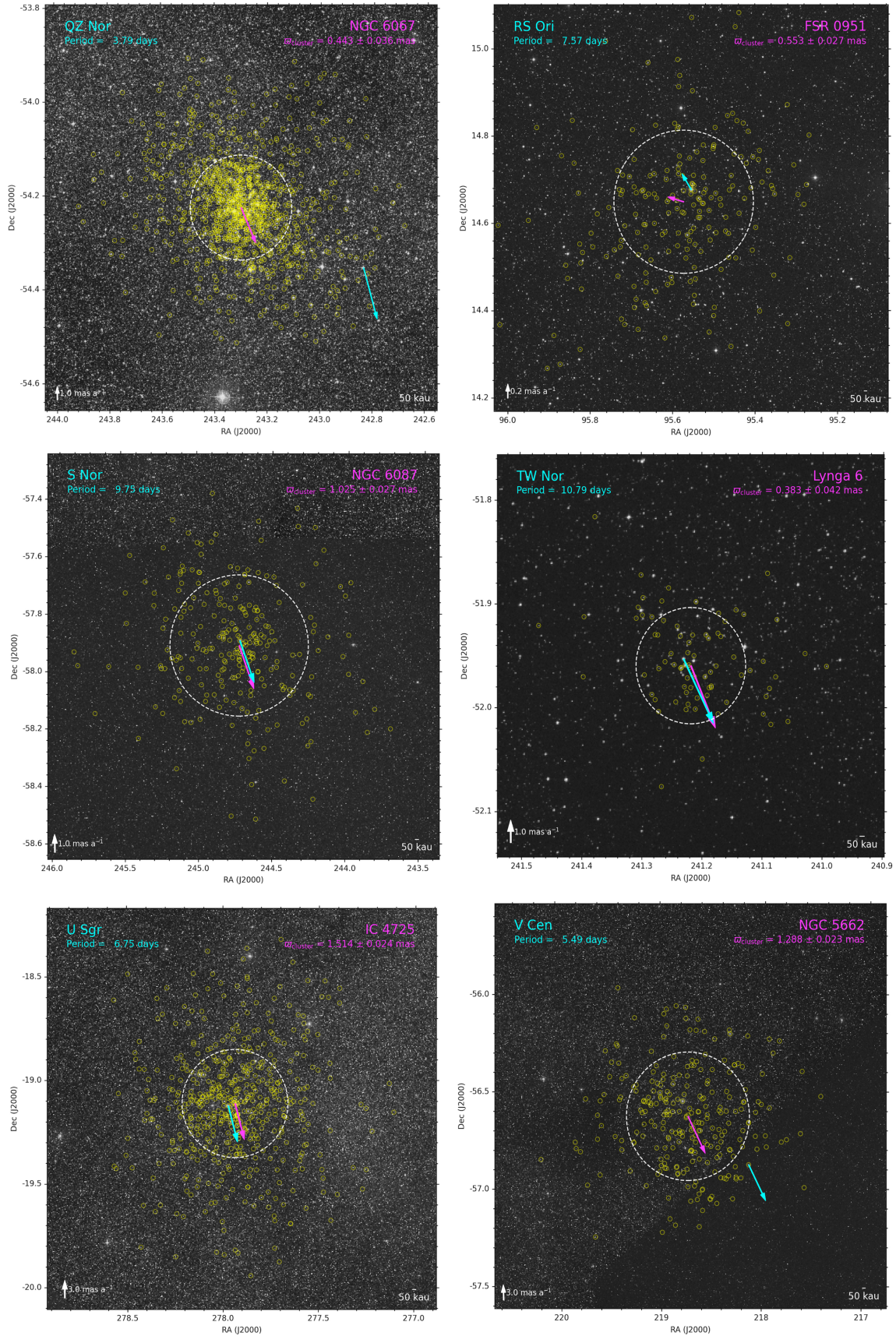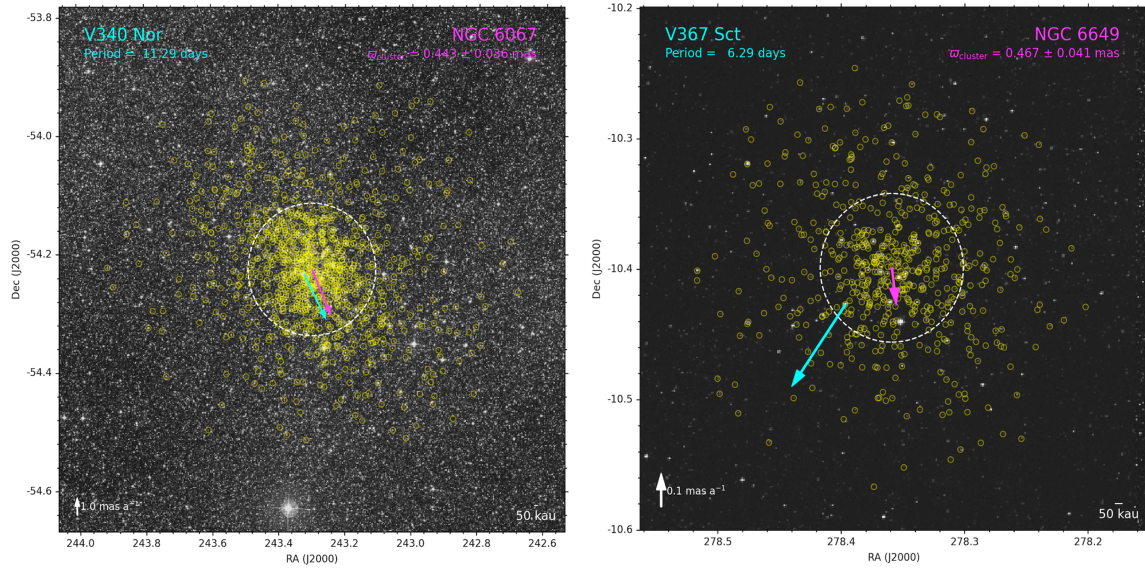
Fig. A.1. continued.

Fig. A.1. continued.